NASA TECHNICAL NOTE

NASA TN D-2119

c. 1

LOAN COPY: RETURN TO
AFWL (WLL—)
KIRTLAND AFB, N MEX

TECH LIBRARY KAFB, NM
0154632

NASA TN D-2119

ONE-DIMENSIONAL HEAT-TRANSFER ANALYSIS OF THERMAL-ENERGY STORAGE FOR SOLAR DIRECT-ENERGY-CONVERSION SYSTEMS

by Richard R. Cullom, William H. Robbins, and Carroll A. Todd

Lewis Research Center
Cleveland, Ohio

NATIONAL AERONAUTICS AND SPACE ADMINISTRATION • WASHINGTON, D. C. • MARCH 1964

ONE-DIMENSIONAL HEAT-TRANSFER ANALYSIS OF THERMAL-ENERGY STORAGE FOR SOLAR DIRECT-ENERGY-CONVERSION SYSTEMS

SUMMARY

A one-dimensional thermal-energy storage system was analyzed as a time-variant heat conduction problem coupled with a change in state of the conducting medium. Solutions for nondimensional surface temperature and solidification depth are presented in graphic form for various modes of heat transfer from one surface of the material. Solutions were obtained by means of finite-difference equations with the assumption that the material was initially at the fusion temperature. Material property values were assumed constant with temperature, and internal heat generation was not considered. The nondimensional solutions presented in this report can be applied to a wide range of one-dimensional cooling problems where a phase change is involved.

The general solutions were applied to the analyses of thermal-energy-storage systems utilizing silicon and lithium hydride. Analysis showed that the high heat of fusion of a thermal-storage material cannot be fully utilized unless the thermal conductivity is also of a relatively high value to allow the thermal energy to be removed from the liquid-solid interface and conducted to the exterior heat-transfer surface with no excessive temperature drop.

INTRODUCTION

Solar electric power systems that are utilized for auxiliary power on satellites in eclipsed orbits must provide some means for maintaining electrical power during the dark period of an orbit. Photovoltaic space-power systems now in operation use nickel-cadmium electrical storage batteries to provide power during the dark time. In the present state of development these high-cycle-life batteries provide a relatively low specific storage capacity and therefore impose a decided weight penalty on the auxiliary power system. If improvements in the specific storage capacity of batteries are not forthcoming, an alternative means of energy storage should be developed to minimize the overall weight of the solar electric power system.

An alternative method of providing power for the duration of the orbital dark time is to store thermal energy as the latent heat of fusion of a suitable material. In a thermal-energy-storage system, the storage material is melted by radiation from the sun, and then, during the shaded portion of the orbit, the

latent heat of fusion is withdrawn and directed to the energy-conversion device. Several solar-powered auxiliary systems have been designed that utilize thermal-energy storage because the relatively high specific storage capability results in a reduction in the overall weight of the auxiliary power system. As a solution to the energy-storage problem, the thermal-storage technique is applicable to thermionic, thermoelectric, or thermodynamic engine auxiliary power systems.

Solutions to the transient heat-transfer process that occurs during the extraction of heat from a melted storage material will aid greatly in the design and estimation of performance of thermal-storage systems. Difference solutions for transient heat conduction with a change of phase of the one-dimensional conducting medium were developed in this analysis. Nondimensional solutions were obtained for a range of time, various storage material properties, and several modes of heat extraction from the storage material. A specific case of the analytical solutions obtained in this report compared quite favorably with an electric analogue solution from reference 1. The solutions presented herein can also be applied to general one-dimensional problems of cooling materials where a phase change is involved.

ANALYSIS

The thermal-storage system is considered herein as a one-dimensional, time-variant, heat-conduction problem coupled with a change in state of the conducting medium (fig. 1). The thermal-storage material is assumed to be semi-infinite with the heat being withdrawn in the x-direction perpendicular to the $x = 0$ plane and with the remaining surfaces being perfectly insulated. The storage-material properties are invariant with temperature. With these assumptions, the the transient heat-conduction equation is

$$\frac{\partial T}{\partial t} = \alpha \frac{\partial^2 T}{\partial x^2} \tag{1}$$

(Symbols are defined in the appendix.) The boundary conditions for the thermal-storage model (fig. 1) are established as follows. Initially, the complete volume of heat-storage material is assumed to be in the liquid phase and at the fusion temperature:

$$T = T_f \qquad \text{and} \qquad l = 0 \qquad \text{at} \quad t = 0$$

As thermal energy is extracted from the storage material, the liquid phase, which is assumed to be continually in intimate contact with the interface, solidifies, and the solid-liquid interface moves in the positive x-direction. At the interface, the temperature is equal to the fusion temperature:

$$T = T_f \qquad \text{at} \quad x = l$$

In a heat balance at the solid-liquid interface, the rate at which the heat of fusion is liberated by the solidifying material is equal to the rate at which heat is transferred from the interface into the solidified phase:

$$\rho_{sol} f \frac{dl}{dt} = -k \frac{\partial T}{\partial x} \qquad \text{at} \quad x = l$$

The rate at which heat is transferred from the $x = 0$ plane must be specified. This boundary condition for the heat-rejection rate can be written in general terms of the surface temperature at $x = 0$ as

$$q = CT_s^n$$

By specification of the proper values of C and n, various modes of heat rejection from the surface can be represented. For example, if the heat transfer to a conversion device is by radiation, $C = \epsilon\sigma$ and $n = 4$. A heat balance at the surface of the storage material yields

$$-k \frac{\partial T}{\partial x} = CT_s^n \qquad \text{at} \quad x = 0$$

Equation (1) may be nondimensionalized by expression of the variables in terms of the following dimensionless parameters:

$$\varphi^n = \left(\frac{T}{T_f}\right)^n$$

$$\tau = \frac{\left(CT_f^{n-1}\right)^2 \alpha t}{k^2}$$

$$X = \frac{CT_f^{n-1} x}{k}$$

The resulting form of the heat-conduction equation is

$$\frac{\partial \varphi}{\partial \tau} = \frac{\partial^2 \varphi}{\partial X^2} \tag{2}$$

Solution of the Heat-Conduction Equation

The solution is effected by the method of the heat-balance integral approximation (ref. 2). In order to obtain the time dependence of the temperature distribution φ that must satisfy the heat-conduction equation, the conduction equation is integrated from 0 to L, which results in a nonlinear differential equation in L

$$\int_0^L \frac{\partial^2\varphi}{\partial X^2}\, dX = \int_0^L \frac{\partial\varphi}{\partial\tau}\, dX \tag{3}$$

or

$$\left.\frac{\partial\varphi}{\partial X}\right|_{X=L} - \left.\frac{\partial\varphi}{\partial X}\right|_{X=0} = \int_0^L \frac{\partial\varphi}{\partial\tau}\, dX \tag{4}$$

The boundary conditions for equation (2) established previously can be summarized in nondimensional form:

$$\varphi = 1 \quad \text{and} \quad L = 0 \quad \text{at} \quad \tau = 0 \tag{5}$$

$$L > X > 0 \quad \text{at} \quad \tau > 0 \tag{6}$$

$$\varphi = 1 \quad \text{at} \quad X = L \tag{7}$$

$$\frac{\partial\varphi}{\partial X} = F\,\frac{dL}{d\tau} \quad \text{at} \quad X = L \tag{8}$$

$$\frac{\partial\varphi}{\partial X} = \varphi^n \quad \text{at} \quad X = 0,\ n = 1, 2, 3, \ldots \tag{9}$$

where the dimensionless solidification depth is defined as

$$L = \frac{cT_f^{n-1}l}{k}$$

and the dimensionless heat of fusion is

$$F = \frac{f}{cT_f}$$

The temperature distribution is assumed to be

$$\varphi(X,\tau) = \chi(\tau) + \psi(\tau)X + \omega(\tau)X^2 \tag{10}$$

Substitution of relation (10) into equations (7) to (9) gives

$$\chi + \psi L + \omega L^2 = 1 \tag{11}$$

$$\psi + 2\omega L = F\,\frac{dL}{d\tau} \tag{12}$$

$$\psi = \chi^n \tag{13}$$

Now, utilization of relations (4) to (12) gives

$$\left.\frac{\partial\varphi}{\partial X}\right|_{X=L} = F\,\frac{dL}{d\tau} \tag{14}$$

$$\left.\frac{\partial\varphi}{\partial X}\right|_{X=0} = \varphi^{n}_{X=0} = \chi^{n} \tag{15}$$

$$\frac{\partial\varphi}{\partial\tau} = \frac{d\chi}{d\tau} + \frac{d\psi}{d\tau}\,X + \frac{d\omega}{d\tau}\,X^{2} \tag{16}$$

Substitution of equations (14) to (16) into relation (4) gives the required differential equation

$$F\,\frac{dL}{d\tau} - \chi^{n} = L\,\frac{d\chi}{d\tau} + \frac{L^{2}}{2}\,\frac{d\psi}{d\tau} + \frac{L^{3}}{3}\,\frac{d\omega}{d\tau} \tag{17}$$

From equations (11) to (13), the coefficients χ, ψ, and ω can be regarded as functions of $L(\tau)$. The introduction of the equations (14) to (16) into equation (17) reduces it to a nonlinear algebraic relation in L_i, where

$$L_i = L(\tau_i) \qquad \text{and} \qquad \tau_i = i\,\Delta\tau \qquad i = 1, 2, 3, \ldots$$

$$(L_i - L_{i-1})F - \Delta\tau\chi_i^{n} = (\chi_i - \chi_{i-1})L_i + \frac{\psi_i - \psi_{i-1}}{2}\,L_i^{2} + \frac{\omega_i - \omega_{i-1}}{3}\,L^{3} \tag{18}$$

The solution of equation (18) yields the desired temperature distribution at discrete values of τ.

The case wherein $n = 1$ and $F = 0.1$ was compared with results obtained with an analogue computer (ref. 1), and values were observed to vary no more than 1 percent for $0 < \tau < 1000$.

Range of Variables

Solutions for dimensionless temperature φ and dimensionless depth of solidification L were obtained as dimensionless time τ was varied from 0.01 to 1000. The dimensionless temperature and depth were calculated over this variation of time for values of dimensionless heat of fusion of 0.1, 0.25, 0.5, 1, 2, 5, 10, and 25. The calculations were made over these ranges of time and heat of fusion for various modes of heat transfer from the storage material as denoted by the cases $n = 1$, 2, 3, 4, and 15.

RESULTS AND DISCUSSION

General Solutions

The results of the analysis are presented in the form of nondimensionalized

curves so that the solutions can be easily applied over a wide range of operating conditions and material properties. In figure 2, the dimensionless temperature φ_s of the surface through which the heat was removed from the energy-storage material is plotted against the dimensionless time τ for a range of dimensionless heats of fusion and various modes of heat removal. The dimensionless depth of solidification L of the energy-storage material is plotted against the dimensionless time τ in figure 3 for several values of dimensionless heat of fusion and for differing methods of heat transfer.

Utilization of figures 2 and 3 necessitates the choice of a thermal-storage material, a specific orbital dark time, and a method of heat transfer from the storage material to an energy-conversion device. To obtain the storage-material surface temperature φ_s at the end of a specified dark time, the dimensionless time τ must be calculated from the orbit dark time, the method of heat transfer, and the storage-material thermal properties. The dimensionless heat of fusion F is then calculated from the thermal properties of the heat-storage material. With the values of dimensionless time and heat of fusion, the n plot (fig. 2) corresponding to the specified mode of heat transfer from the storage material is entered, and the dimensionless temperature is read directly. The absolute temperature of the storage-material surface is then obtained by multiplication of the dimensionless temperature φ_s by the fusion temperature of the heat-storage material. The solutions for dimensionless depth of solidification (fig. 3) are obtained in a similar manner and are dimensionalized with the proper group of material properties.

Analysis of Thermal-Storage System

Application of general solution with $n = 1$. - An analysis of thermal-energy-storage systems was made with the solutions of figures 2 and 3 over a range of initial rates of heat rejection from the storage material to an energy-conversion device. Silicon and lithium hydride were chosen as storage-material examples to supply thermal energy to a conversion device for a dark time of 1/2 hour by forced convection, approximated by the case $n = 1$. Material properties shown in table I were obtained from references 3 and 4. The rejection heat-transfer coefficient was constant with time and was specified by the initial heat-rejection rate and the fusion temperature. The dimensionless temperature of the storage-material surface at the end of the 1/2-hour dark time is shown in figure 4(a) for the silicon system as well as the lithium hydride system. As the initial heat-rejection rate increased, the surface temperature at the end of the dark time decreased, as expected. The final surface temperature of the lithium hydride thermal-storage system decreased more rapidly with initial heat-rejection rate than the corresponding temperature of the silicon system. Because the surface temperature and the heat-rejection rate are proportionally related by $q = AT_s^n$ (for $n = 1$), the value of the temperature ratio at the end of the dark time shown in figure 4(a) is also the ratio of the final heat-rejection rate to the initial heat-rejection rate for a constant heat-transfer coefficient. Thus, as the initial heat-rejection rate increased, the ratio of the heat-transfer rate available at the end of the dark time to the initial heat-rejection rate decreased. At the end of the 1/2-hour dark time the heat-transfer rate available

from the silicon storage system as well as the lithium hydride storage system had decreased to 0.9 and 0.37, respectively, of the initial heat-rejection rate of 20 watts per square centimeter. Even though lithium hydride displays a relatively high heat of fusion, greater than that of silicon, apparently the relatively lower thermal conductivity of the solid-phase lithium hydride determined the low final surface temperature and, hence, the low final heat-transfer rate. It is concluded, therefore, that the choice of a heat-storage material cannot be based on heat of fusion alone, but the solid-phase thermal conductivity, among other properties, must also be considered.

The depth of solidification of the silicon storage material increased with initial heat-rejection rate (fig. 4(a)), as expected. Over the range of rejection rates investigated, it appeared that the thickness of silicon required to store the amount of thermal energy specified by the initial rejection rate was reasonable. The depth of solidification of the lithium hydride increased as the value of the heat-rejection rate increased to approximately 40 watts per square centimeter; then the depth only slightly increased as the heat-rejection rate increased further. The low values of lithium hydride solidification depth can probably be attributed to the relatively high value of heat of fusion and the relatively low value of thermal conductivity.

Application of general solution with $n = 15$. - The temperature ratio and the depth of solidification at the end of the 1/2-hour dark time are presented in figure 4(b) for silicon storage material providing energy for a thermionic converter. A thermionic device was analyzed because, as will be shown, the power output is very sensitive to operating temperature level and therefore this system would probably be the most difficult conversion system to provide with thermal-energy storage that in simple form is nonisothermal. The output current of a thermionic device is theoretically predicted by the Richardson-Dushman equation (ref. 5)

$$J = AT_c^2 e^{-b_0/T_c}$$

where A is a constant equal to 120.4 amperes per square centimeter per $^{\circ}R^2$, T_c the absolute cathode surface temperature, and b_0 the temperature equivalent of the cathode work function. From this equation it can be seen that the thermionic power output is an exponential function of the surface emitting temperature. In a thermionic converter system where the cathode is directly attached to the storage material, the energy-rejection rate from the storage material is also a very strong function of the storage-material surface temperature, the temperature exponent, approximated from the Richardson-Dushman equation, being of the order of 15. The heat-rejection rate, therefore, which is a function of the surface temperature to an exponent, will decrease very rapidly from its initial value as the surface temperature decreases. Then, for a given initial heat-rejection rate, the surface temperature at the end of the dark time will be higher for the thermionic system (fig. 4(b)) than for the convective system (fig. 4(a)) because the thermionic heat-rejection rate decreases more rapidly from its initial value; the average heat rejection rate and, hence, the total amount of heat rejected during the dark time is, thus, lower for the $n = 15$ case. Because the solidification depth is also a function of the total amount of heat rejected over the

dark time, the solidification depth for the thermionic system will be lower (fig. 4(b)) than that for the convective system (fig. 4(a)).

The theoretical performance of a solar thermionic converter that utilized thermal-energy storage during 1/2 hour of dark time is shown in figure 5. The variation of power output with dark time is presented for three initial power output levels. The power levels, as computed from the Richardson-Dushman equation, correspond to initial cathode temperatures of approximately 1500°, 1600°, and 1700° K; thus, it is assumed that there are varying temperature differences between the storage-material surface and the cathode emitting surface of approximately 10, 5, and 0 percent of the fusion temperature. The cathode material was assumed to be thoriated tungsten operating at a net potential difference of 1.5 volts. The process of removing thermal energy from the storage material and converting it into electrical energy is assumed to have an initial overall efficiency of 10 percent. For the cases of a finite temperature difference, the assumption was made that the cathode surface temperature decreased with time in proportion to the surface temperature of the thermal-storage material. The theoretical power output of the thermionic devices, according to the Richardson-Dushman equation, decreased rapidly with time because of the exponential variation in current output with emission temperature. At the end of the 1/2-hour dark time, the specific power output of the thermionic devices was approximately 10 percent of their respective initial power output.

EVALUATION AND DISCUSSION OF PHYSICAL PROPERTIES

To determine which material properties are of importance in the thermal-energy-storage process, it was necessary to evaluate the material properties individually to ascertain their effect on the system parameters of ratio of final to initial surface temperature and storage-material solidification depth. With utilization of solutions obtained from figure 2, the sensitivity of the temperature ratio to the material properties was investigated by independently varying the material properties. This investigation showed that the temperature ratio was equally affected to the greatest extent by the material solid-phase density and the thermal conductivity. The latent heat of fusion followed closely as the next most important property. The specific heat was much less important.

Thus, a high value of solid-phase thermal conductivity, as well as a high value of heat of fusion, is required for an efficient thermal-energy-storage system.

The one-dimensional analysis indicates that heat-storage capacity can be severely limited by the thermal conductivity of the solid phase. This limitation can be relieved somewhat when the thermal-storage process in the actual three-dimensional case is considered. An example of a three-dimensional configuration is a closely coiled tube that is buried within the storage medium. A heat-transfer fluid flows inside the tube to remove the thermal energy rejected by the storage material. If the coil spacing is determined to be twice the solidification depth, as computed from the one-dimensional relations, effective heat storage can be achieved even with lithium hydride. This technique has been used in the design of a solar-heated mercury boiler (Sunflower Project).

Other techniques make use of fins, rods, and wire gauze fabricated of materials with high thermal conductivity.

CONCLUDING REMARKS

This analysis considered the system as a one-dimensional, time-variant, heat-conduction problem coupled with a change in state of the conducting medium. Solutions for nondimensional surface temperature and solidification depth were obtained and are presented as functions of time in graphic form for various mode of heat transfer from the material surface. Solutions were obtained by means of finite-difference equations assuming the material to be initially at the fusion temperature. Material property values were assumed constant with temperature, and internal heat generation was not considered. The nondimensional solutions presented in this report can be applied to a wide range of one-dimensional cooling problems where a phase change is involved.

Analysis of these general solutions, as applied to the thermal-energy-storage component of solar direct-energy-conversion systems, indicates the following. The high heat of fusion of a thermal-storage material cannot be fully utilized unless the solid-phase thermal conductivity is of sufficient magnitude to allow the thermal energy to be removed from the liquid-solid interface and conducted to the exterior heat-transfer surface with no excessive temperature drop.

Lewis Research Center
National Aeronautics and Space Administration
Cleveland, Ohio, October 2, 1963

APPENDIX - SYMBOLS

A	constant, 120.4 amp/(sq cm)($^{\circ}R^2$)
b_0	temperature equivalent of cathode work function
C	constant, Btu/(sq in.)(sec)($^{\circ}R^n$)
c	specific heat, Btu/(lb)($^{\circ}R$)
F	dimensionless heat of fusion, f/cT_f
f	heat of fusion, Btu/lb
i	integer
J	theoretical output current, amp/sq cm
k	thermal conductivity, Btu/(hr)(ft)($^{\circ}R$)
L	dimensionless solidification depth, $CT_f^{n-1}l/k$
l	solidification depth, in.
n	temperature exponent
P	power output, w/sq cm
q	heat-transfer rate, w/sq cm
T	temperature, $^{\circ}R$
t	time, min
X	dimensionless coordinate, $CT_f^{n-1}x/k$
x	coordinate, in.
α	thermal diffusivity, sq ft/hr
ϵ	emissivity
ρ	density, lb/cu ft
σ	Boltzmann's constant
τ	dimensionless time, $\left(CT_f^{n-1}\right)^2 \alpha t/k^2$
φ	dimensionless temperature, T/T_f

χ, ψ, ω coefficients in eq. (10)

Subscripts:

c	cathode
d	dark
f	fusion
i	initial
s	surface
sol	solid phase

REFERENCES

1. Kreith, F., and Romie, F. E.: A Study of the Thermal Diffusion Equation with Boundary Conditions Corresponding to Solidification or Melting of Materials Initially at the Fusion Temperature. Proc. Phys. Soc., pt. 5, vol. 68, no. 425B, May 1, 1955, pp. 277-291.

2. Goodman, T. R.: The Heat-Balance Integral and Its Application to Problems Involving a Change of Phase. ASME Trans., vol. 80, no. 2, Feb. 1958, pp. 335-342.

3. Hodgman, Charles D., ed.: Handbook of Chemistry and Physics. Thirty-eighth ed., Chem. Rubber Pub. Co., 1956-1957.

4. Anon.: Thermal Properties of Solids. Rep. AST-E9R-12073, Chance Vought Aircraft, Inc., Sept. 1, 1959.

5. Spangenberg, Karl R.: Vacuum Tubes. McGraw-Hill Book Co., Inc., 1948.

TABLE I. - PROPERTIES OF THERMAL-

STORAGE MATERIALS

Property	Silicon	Lithium hydride
Fusion temperature, T_f, $^{\circ}R$	3020	1715
Heat of fusion, f, Btu/lb	706	1251
Thermal conductivity, k, Btu/(hr)(ft)($^{\circ}R$)	46.2	2.4
Density, ρ, lb/cu ft	150.0	43.0
Specific heat, c, Btu/(lb)($^{\circ}R$)	0.21	1.9

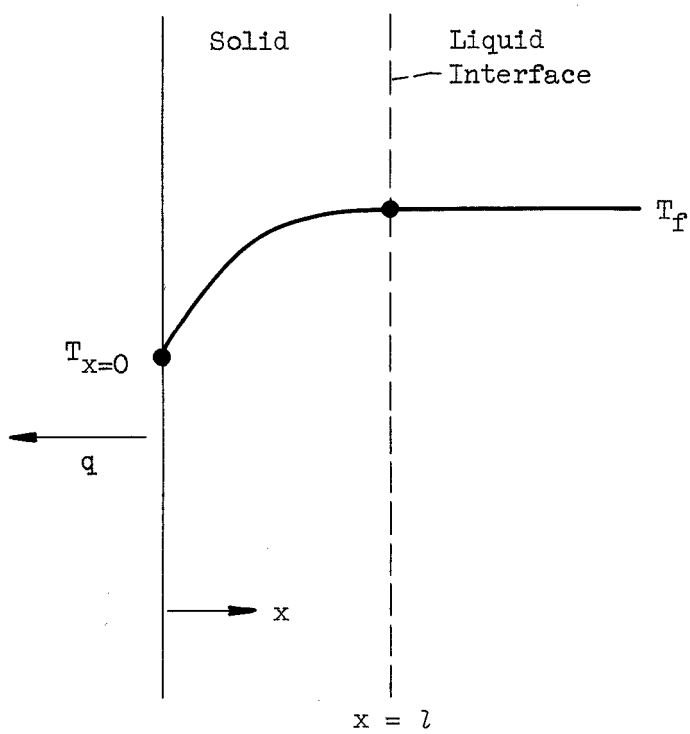

Figure 1. - Thermal-energy-storage model.
Time $t > 0$.

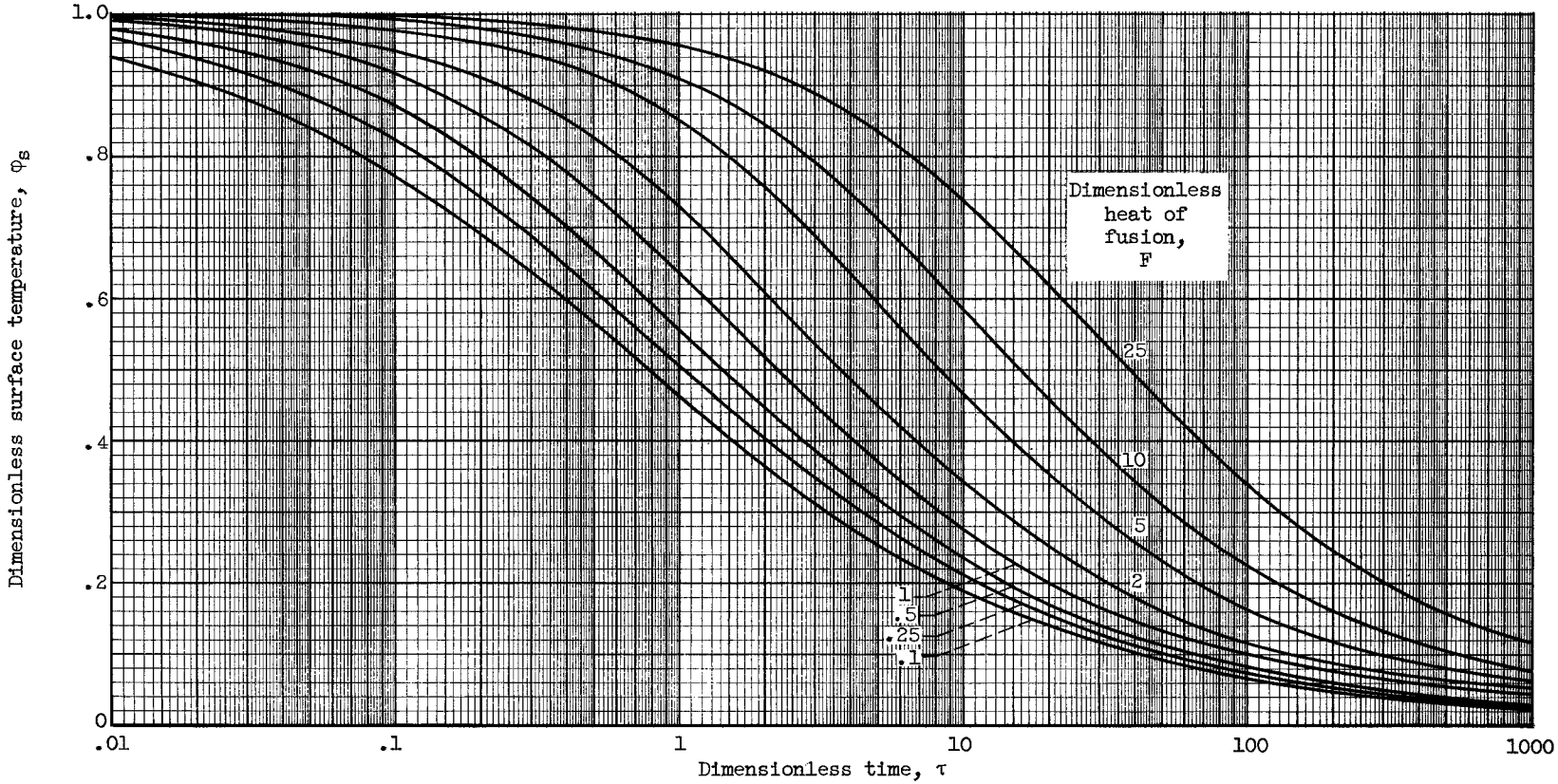

(a) Temperature exponent, 1.

Figure 2. - Time-temperature relations for various dimensionless heats of fusion.

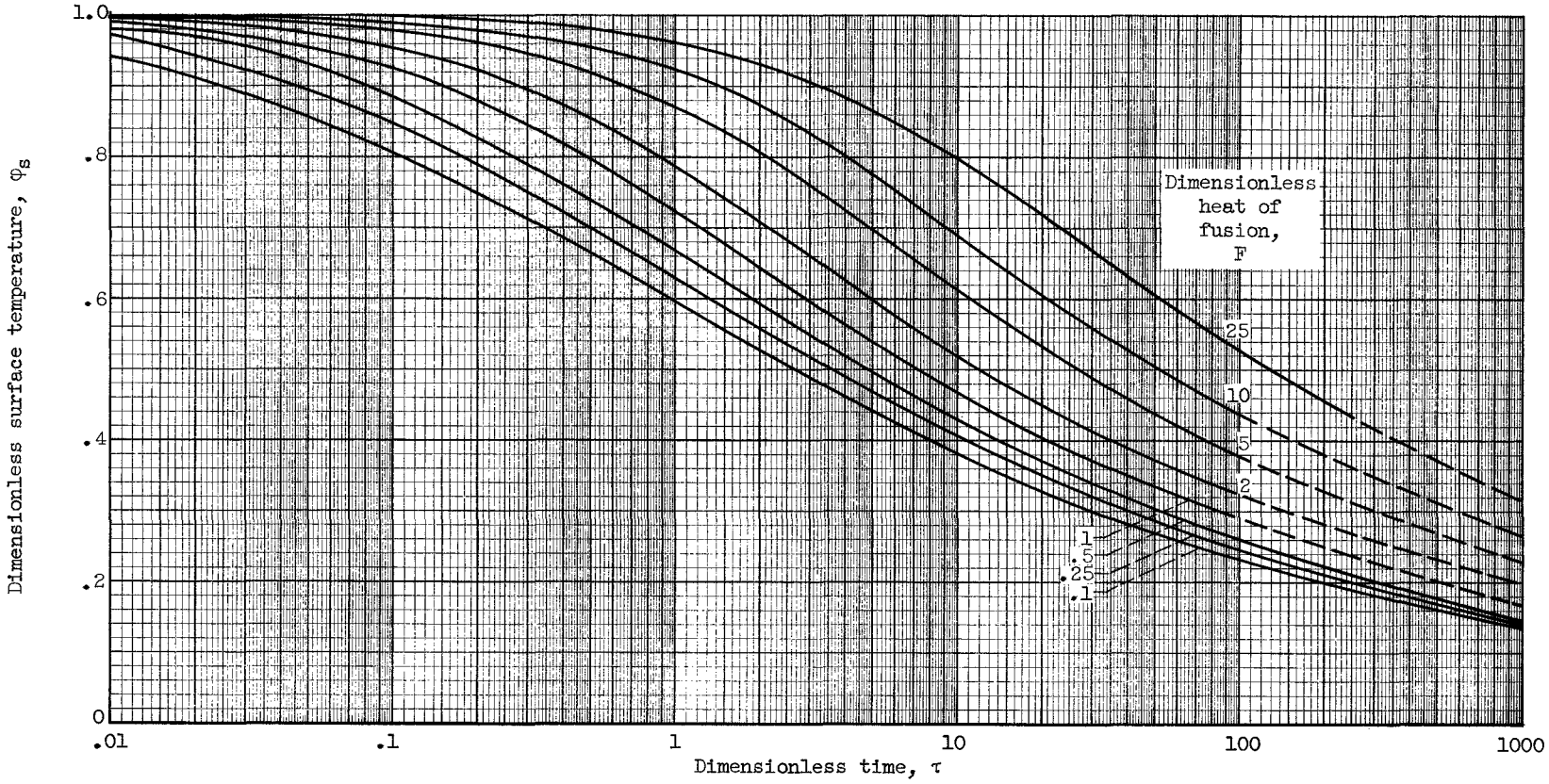

(b) Temperature exponent, 2.

Figure 2. - Continued. Time-temperature relations for various dimensionless heats of fusion.

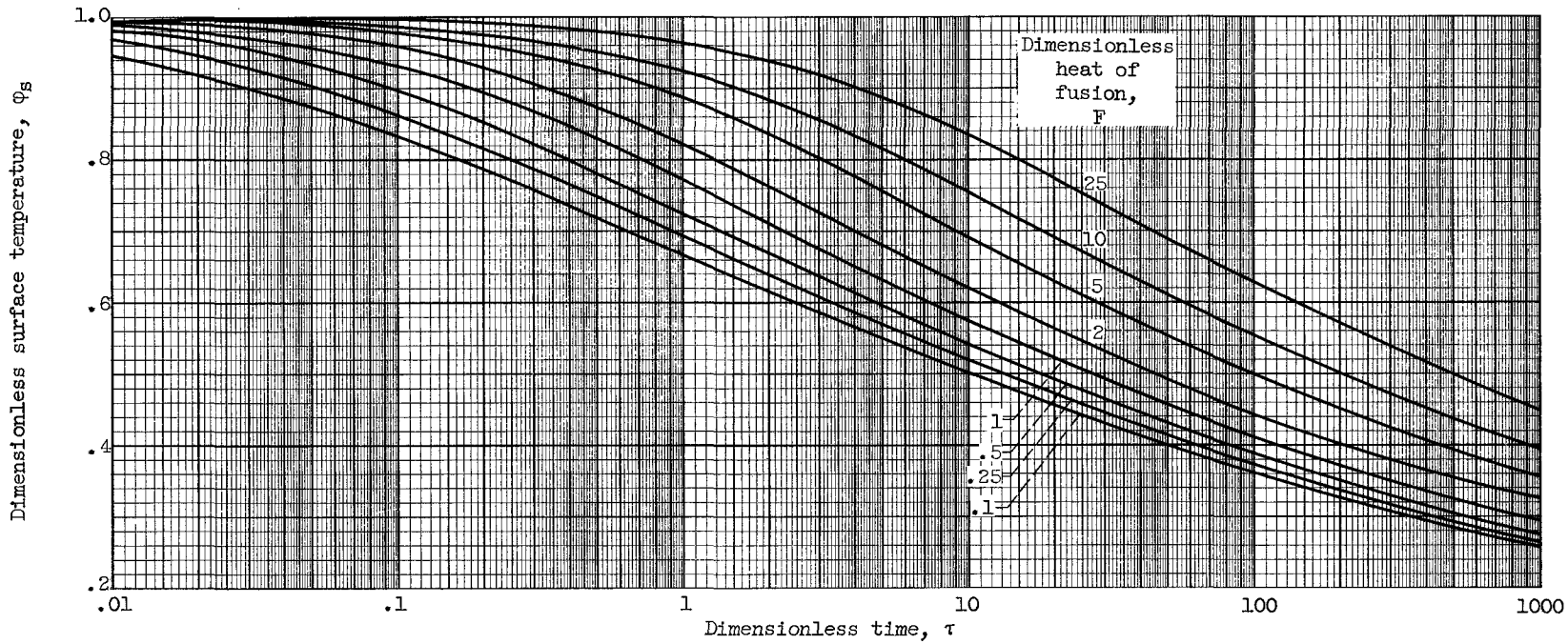

(c) Temperature exponent, 3.

Figure 2. - Continued. Time-temperature relations for various dimensionless heats of fusion.

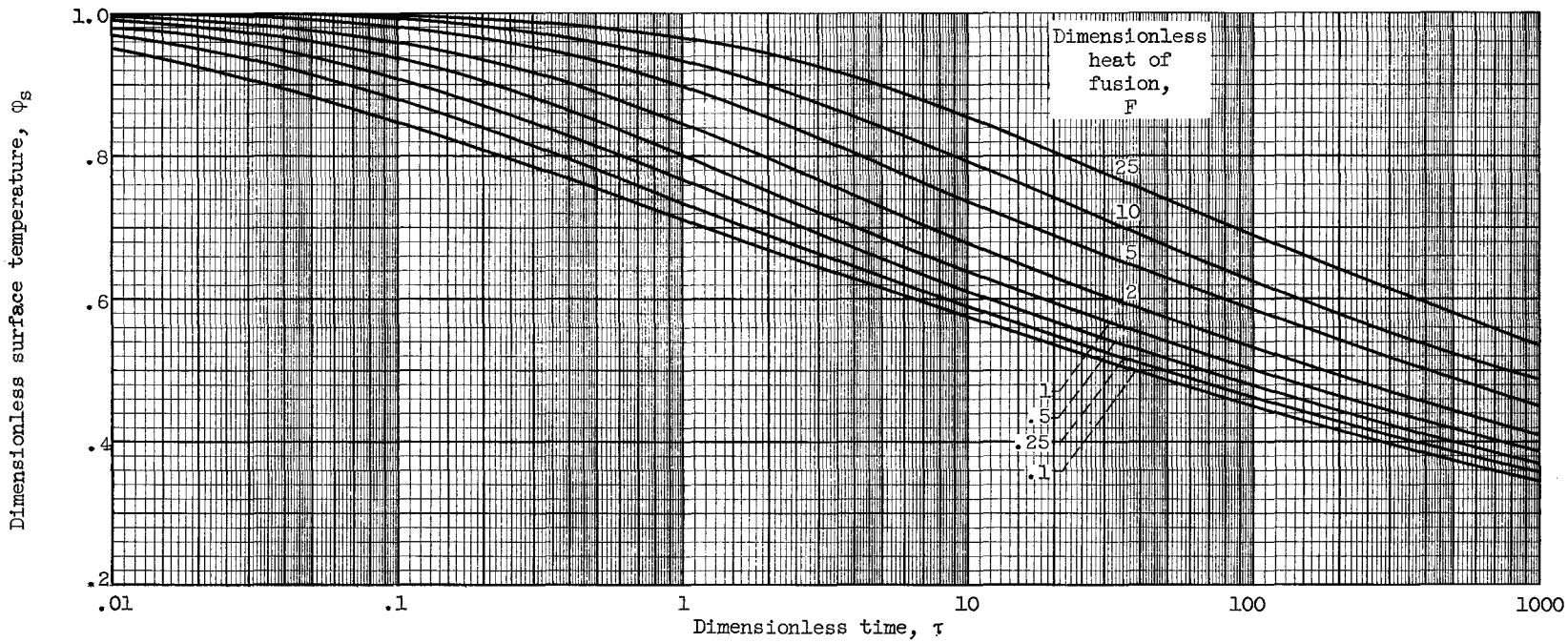

(d) Temperature exponent, 4.

Figure 2. - Continued. Time-temperature relations for various dimensionless heats of fusion.

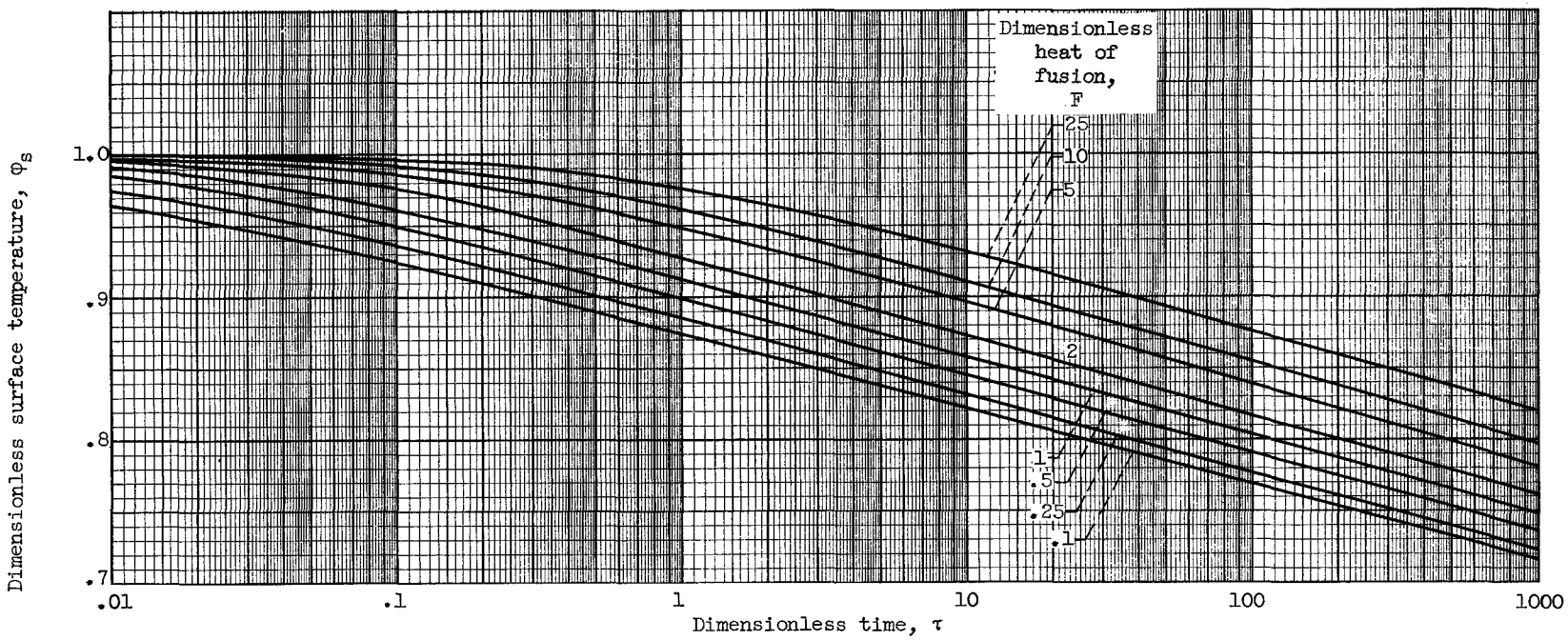

(e) Temperature exponent, 15.

Figure 2. - Concluded. Time-temperature relations for various dimensionless heats of fusion.

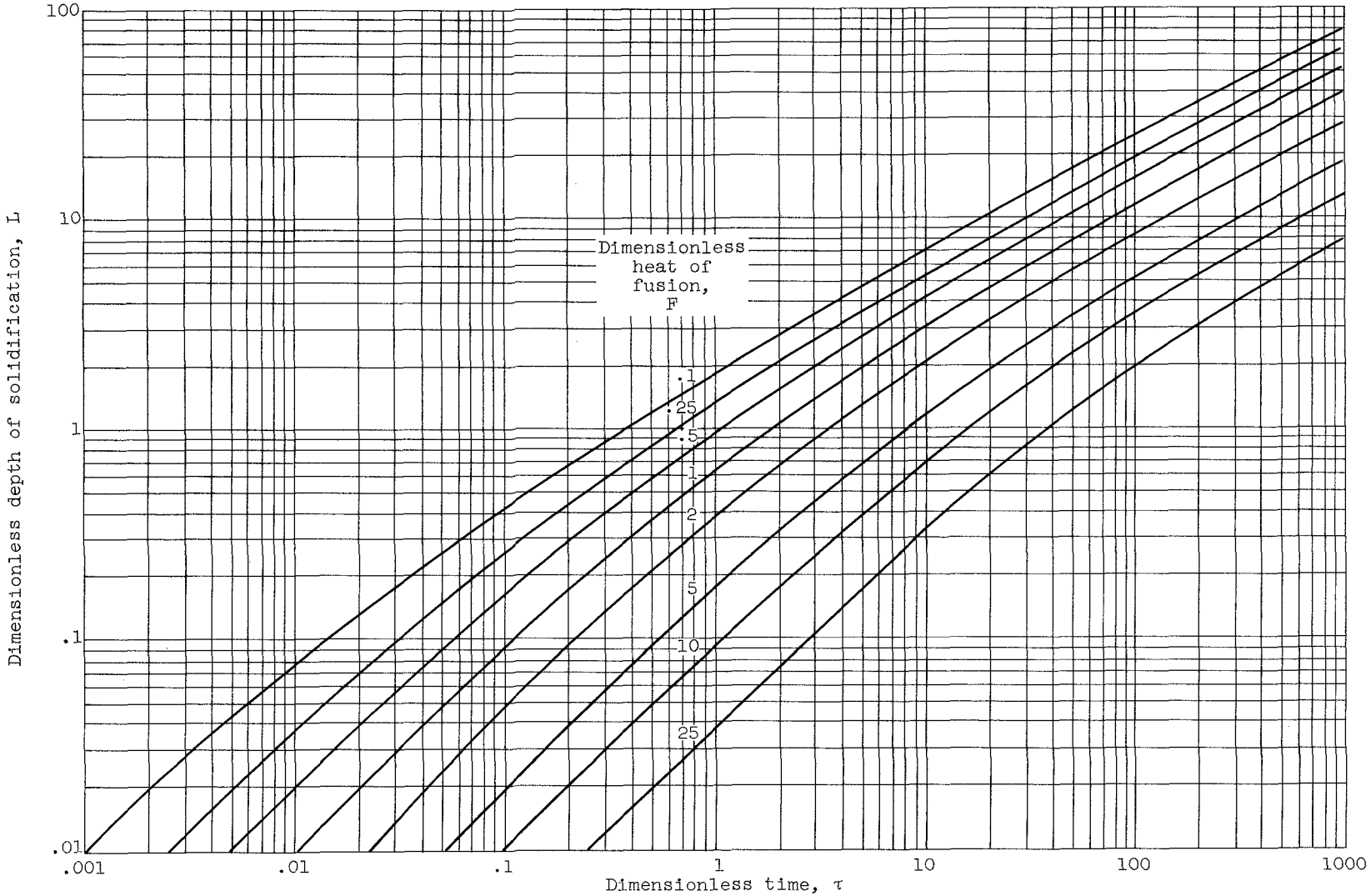

(a) Temperature exponent, 1.

Figure 3. - Time - solidification-depth relations for various dimensionless heats of fusion.

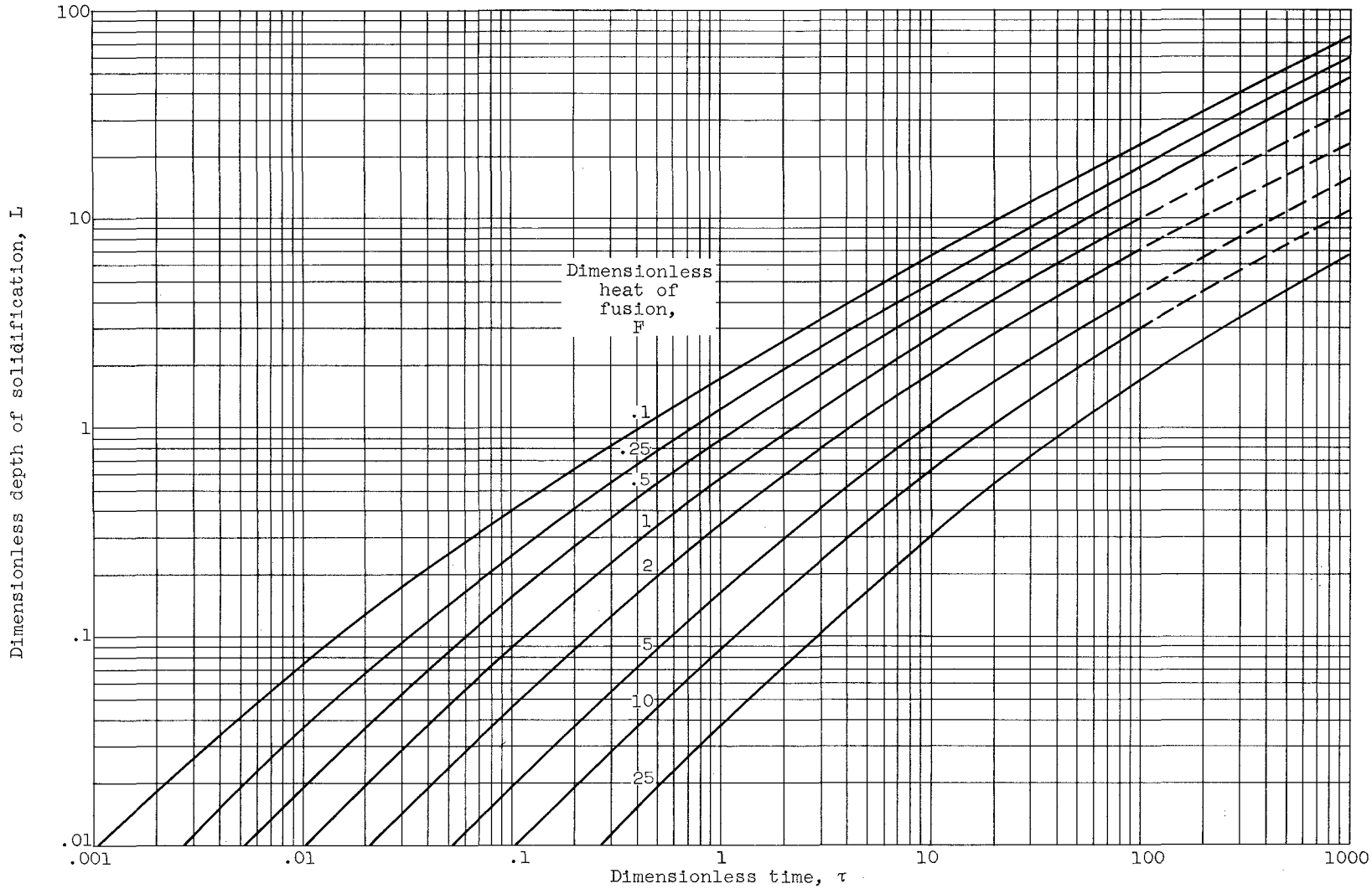

(b) Temperature exponent, 2.

Figure 3. - Continued. Time - solidification-depth relations for various dimensionless heats of fusion.

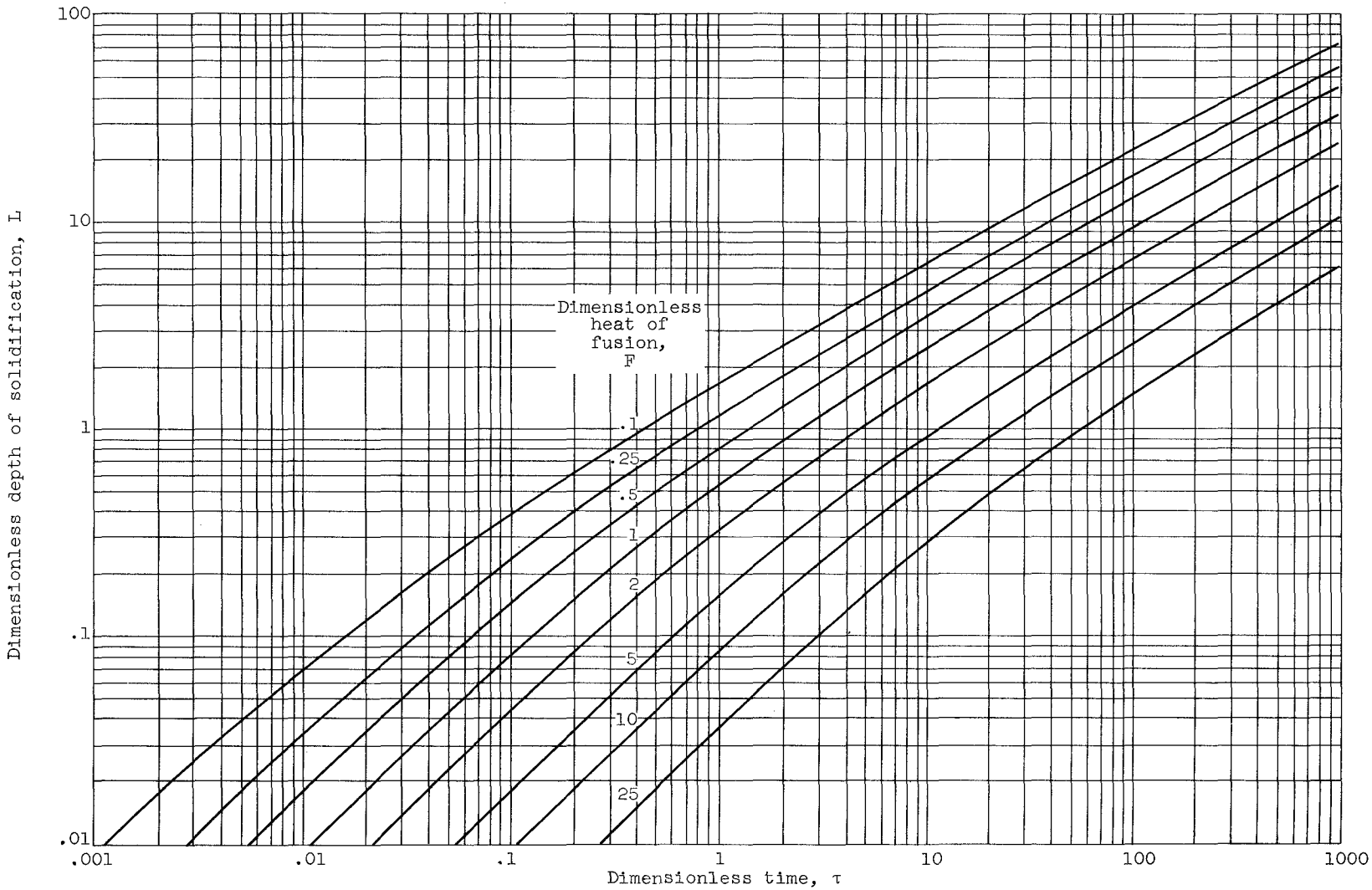

(c) Temperature exponent, 3.

Figure 3. - Continued. Time - solidification-depth relations for various dimensionless heats of fusion.

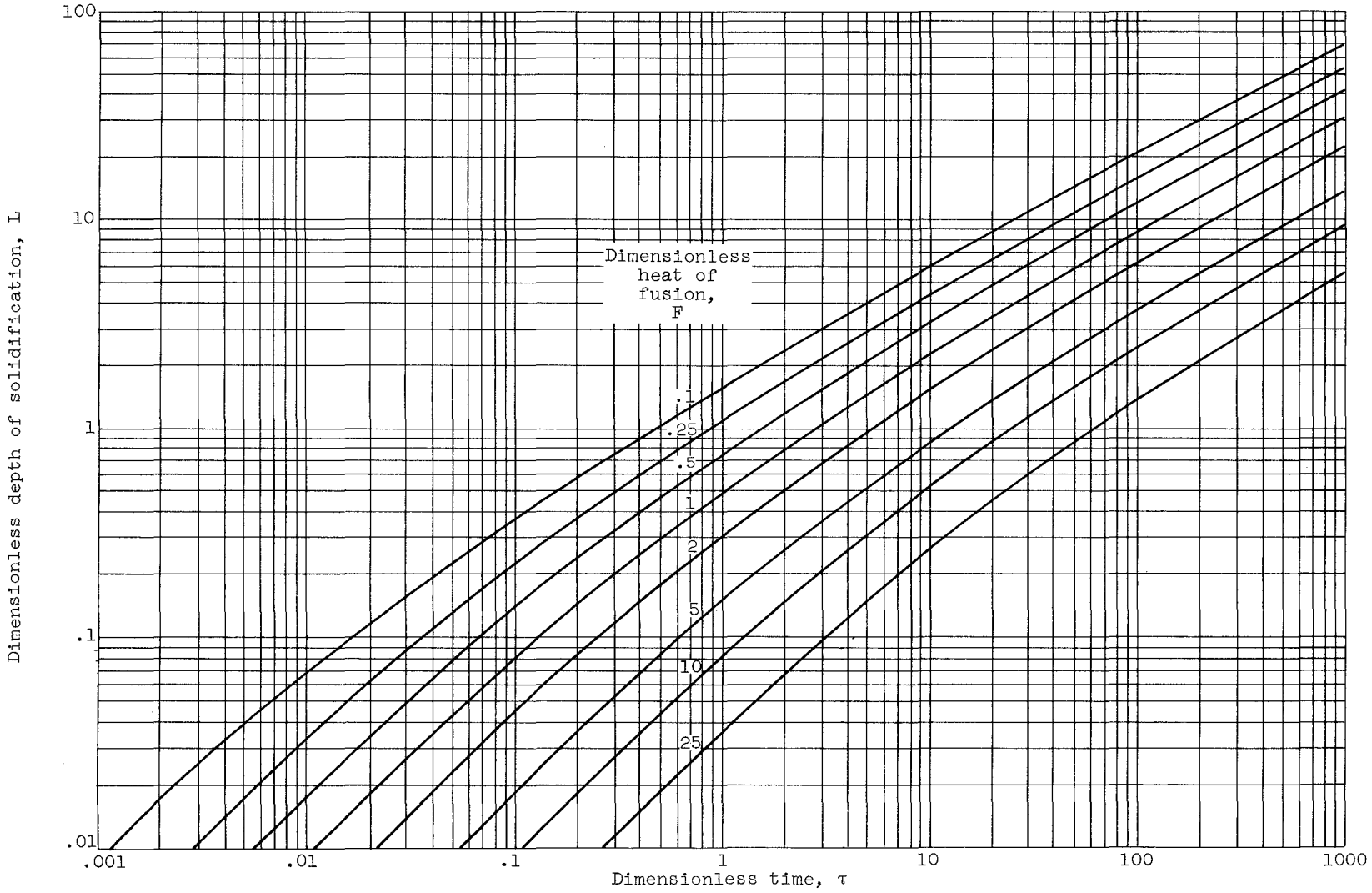

(d) Temperature exponent, 4.

Figure 3. - Continued. Time - solidification-depth relations for various dimensionless heats of fusion.

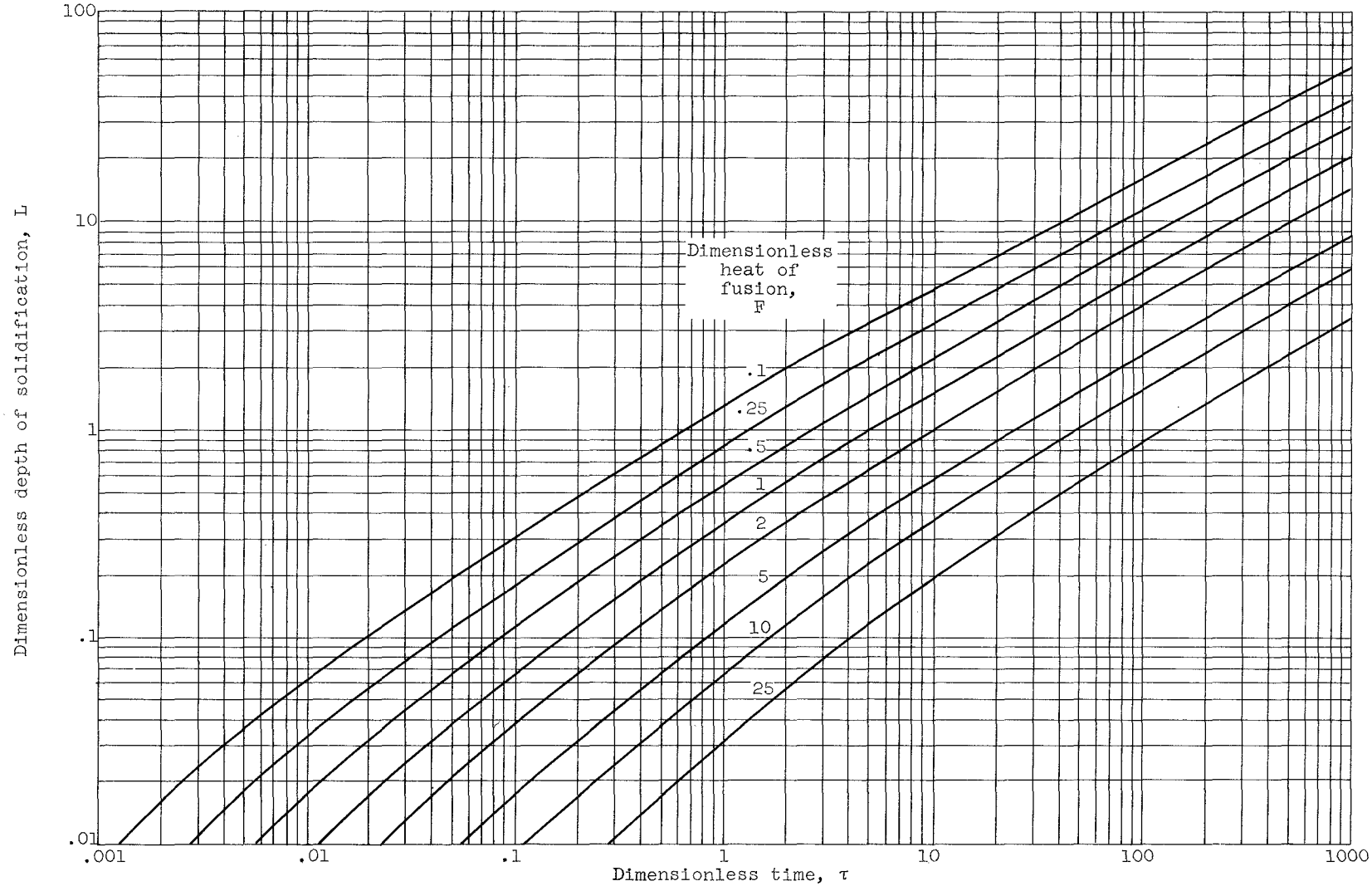

(e) Temperature exponent, 15.

Figure 3. - Concluded. Time - solidification-depth relations for various dimensionless heats of fusion.

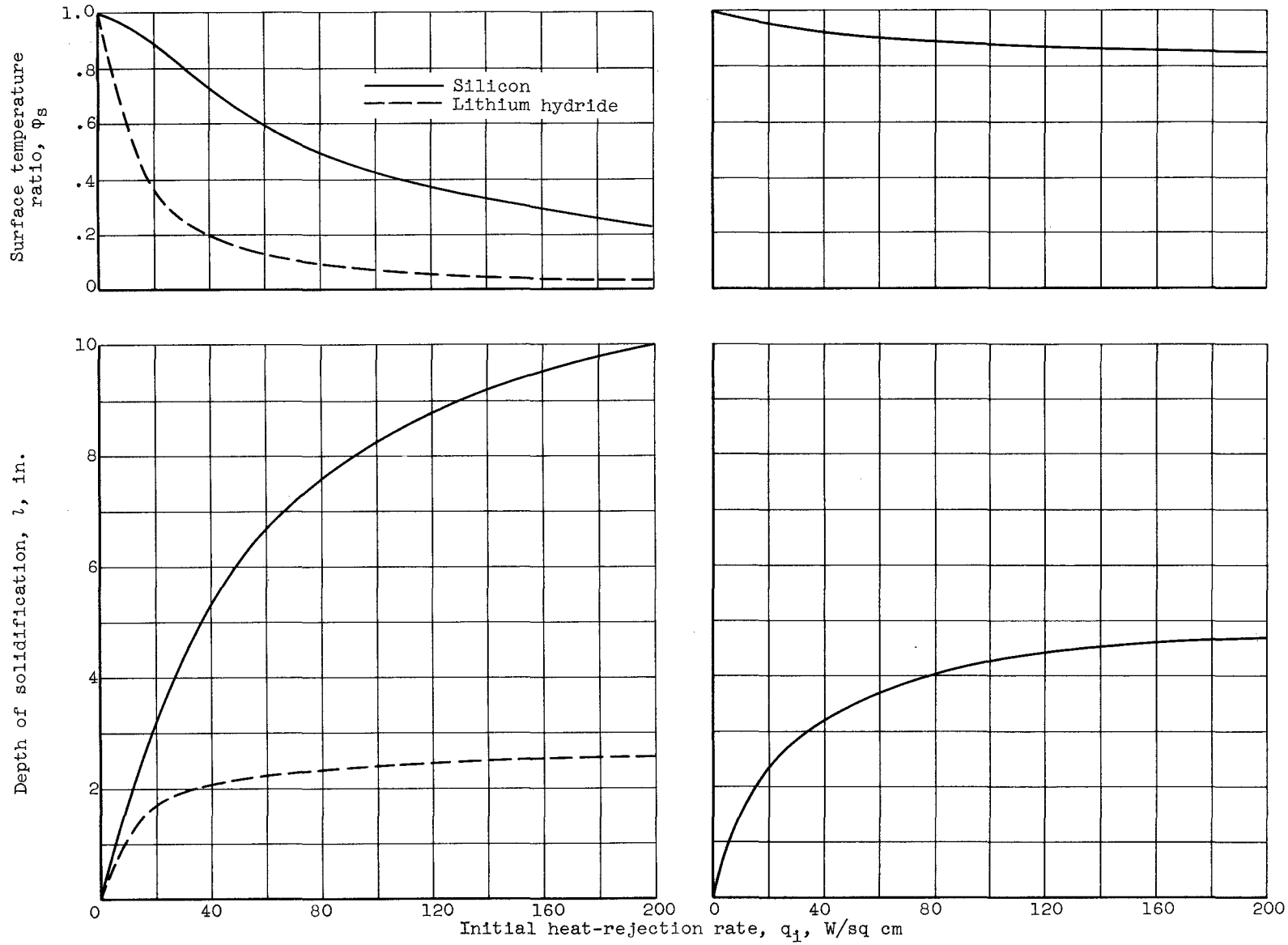

(a) Temperature exponent, 1.

(b) Temperature exponent, 15.

Figure 4. - Temperature ratio and depth of solidification as function of initial heat-rejection rate. Dark time, 1/2 hour.

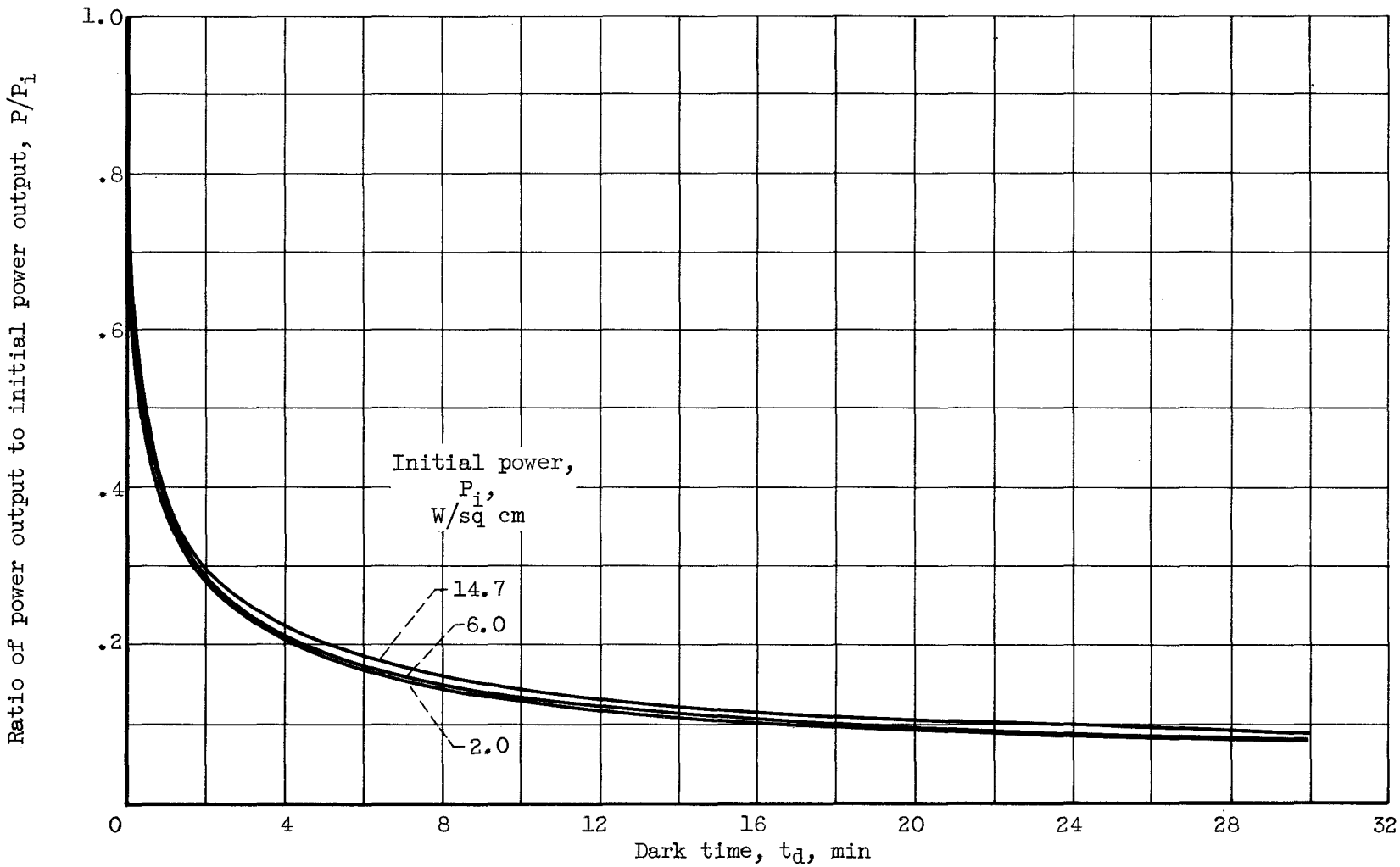

Figure 5. - Power output of thermionic diode as function of dark time for silicon. Temperature exponent, 15.